

Nanopillar Arrays on Semiconductor Membranes as Electron Emission Amplifiers

Hua Qin*, Hyun-Seok Kim, and Robert H. Blick

Department of Electrical and Computer Engineering,

University of Wisconsin-Madison, 1415 Engineering Drive, Madison, WI-53706, USA

(Dated: November 30, 2018)

Abstract

A new transmission-type electron multiplier was fabricated from silicon-on-insulator (SOI) material by integrating an array of one dimensional (1D) silicon nanopillars onto a two dimensional (2D) silicon membrane. Primary electrons are injected into the nanopillar-membrane system from the flat surface of the membrane, while electron emission from the other side is probed by an anode. The secondary electron yield (SEY) from nanopillars is found to be about 1.8 times that of plane silicon membrane. This gain in electron number is slightly enhanced by the electric field applied from the anode. Further optimization of the dimensions of nanopillars and membrane and application of field emission promise an even higher gain for detector applications and allow for probing of electronic/mechanical excitations in nanopillar-membrane system excited by incident particles or radiation.

*Electronic mail: QIN1@WISC.EDU

PACS numbers: 79.20.Hx, 73.30.+y, 61.46.-w, 87.64.Ee, 79.70.+q

The interaction of energetic particles with matter is a fundamental process in physics. Many interaction pathways exist, leading to the production of a variety of secondary particles. Arguably the most important of these processes is the so-called secondary electron emission (SEE), which in addition to its fundamental importance in materials properties also serves as the basis for a broad variety of widely used practical devices (e.g. electron multipliers; cathode ray screens; silicon detectors) [1, 2, 3, 4, 5, 6, 7, 8]. In the case of SEE stimulated by primary electrons, the yield of secondary electrons (SEY) is determined by the balance between two opposing effects: on the one hand, the thicker the layer of material interacting with the primary particles, the greater the probability of an electron-generating event. However, at the same time, as the penetration depth of primary electrons increases the ability of a secondary electron to escape from the material decreases. This determines that SEE is an effect that mainly occurs near the surface and a grazing incident angle produces more secondary electrons [1, 9]. It has been found that a proper surface roughness can enhance SEE while large corrugations suppress SEE. Recently, it has also been found that SEE can be either enhanced or suppressed by carbon nanofibers, depending on whether nanofibers are suspended from or attached to the underlying silicon substrate [10]. Unlike this random configuration of carbon nanofibers or conventional surface roughness produced in a sputtering process for metallic/dielectric material deposition, the advances in nano fabrication and material science now allow for precise engineering of surfaces to optimize SEE and understanding new physics of electron impact on nano objects. Here we demonstrate a nanostructured material consisting of an array of one dimensional (1D) silicon nanopillars fabricated on the surface of a two dimensional (2D) layer of crystalline silicon. It is shown that this juxtaposition of structures of different dimensionalities results in an enhanced SEE response. The choice of a thin membrane allows for a separation of primary and secondary electrons, i.e., a transmission-type electron generation. Naturally, this scheme is easy to extend to other materials with excellent electron emission properties, such as diamond nanopillars, aligned carbon nanotubes and zinc oxide nanowires. This ability to alter fundamental material properties by manipulation of device geometry at the nanoscale level opens new opportunities for exploring electronic and mechanical excitations in nano structures and new designs of novel materials and devices.

For the purpose of this experiment we fabricated several membranes from *n*-type silicon-on-insulator (SOI) wafers, as schematically shown in Fig. 1(a). The starting SOI material

consists of a 3-micron thin layer of silicon on an insulating layer of silicon dioxide ($1.1\ \mu\text{m}$). The substrate is of n -type silicon with a thickness of $725\ \mu\text{m}$. The resistivity of the SOI is of the order of $12\ \Omega \cdot \text{cm}$. Both the SOI and the silicon substrate have a crystal orientation of (100). After the SOI was thinned down to $2.9\ \mu\text{m}$ and thus a $250\ \text{nm}$ layer of silicon dioxide was formed on top by thermal oxidation, the whole wafer was then capped with a thin layer of silicon nitride ($\sim 400\ \text{nm}$) by using low pressure chemical vapor deposition (LPCVD). Being chemically resistive to potassium hydroxide (KOH) solution, the silicon nitride coating provides an etch mask in an anisotropic etching of silicon to form thin silicon membranes. The final membranes of square shape have a side length of $35\ \mu\text{m}$. On each device 16 such identical membranes were fabricated into four 2×2 arrays. A scanning electron micrograph of four such membranes is shown in Fig. 1(b). On each membrane, an array ($\approx 17,600$) of round nanopillars was fabricated from the membrane host by electron-beam lithography (EBL), gold deposition and a successive reactive-ion etching (RIE). Finally, the gold mask was removed in a wet chemical etch step, leaving clean silicon nanopillars on the membranes. Each pillar has a diameter of $80\ \text{nm}$ and a height of $300\ \text{nm}$. Close-ups of nanopillar arrays with a pitch of $200\ \text{nm}$ are shown in Fig. 1(c) and (d). In Fig. 1(e), the SEM graph of a cleaved membrane reveals the overall architecture of one-dimensional nanopillars placed on the two-dimensional membrane. Also indicated in Fig. 1(b) is that the nanopillars are patterned in a frame marked Δ around the center piece of the plain membrane marked M. This allows to discriminate electron transmission through the membrane alone (M), the nanopillar-membrane system (Δ), and through the bulk material (B) which includes two extra layers of dielectrics. The thickness of membrane (M) is about $1.6\ \mu\text{m}$.

The experimental setup we used is also shown schematically in Fig. 1(a): the device is mounted in a scanning electron microscope (SEM) which provides a vacuum environment ($p \sim 10^{-6}\ \text{mbar}$) and most importantly a controllable electron beam (e-beam). The e-beam is scanned over the backside of the membrane to inject electrons in the energy range of $E_p = 1 - 30\ \text{keV}$. The membrane is connected to an electron reservoir at ground potential. A large anode is placed above the nanopillars, providing an extraction or retarding voltage for electrons emitted from the membrane and nanopillars. Most importantly, the anode is designed as a Faraday cup such that the efficiency of collecting electrons approaches 100%. By controlling the anode voltage (V_a) while monitoring the anode current (I_a), secondary electron emission ($E \lesssim 50\ \text{eV}$) can be differentiated from electrons transmitted through

the membrane ($E \leq E_p$) [1] or from field emitted electrons [11]. This provides a simple method to analyze the energy distribution of emitted electrons and allows for identifying the effect of nanopillars on electron emission. This experimental setup is similar to a scanning transmission electron microscope (STEM) [12, 13]. However, the aim here is not to obtain an atomic resolution which requires an ultra-thin membrane. The experimental results shown below will demonstrate that electron emission is enhanced by introducing nanopillars on the exit side of a thin membrane.

Fig. 1(f) shows a Monte-Carlo simulation revealing the spatial distribution of primary electrons (colorized dots) entering from below and the SEE (gray scale in red color) in a nanopillar-membrane device. In the simulation, the real dimensions were used for the nanopillar. The membrane thickness was chosen to be same as the height of the nanopillar to reduce the simulation time. The electron energy was set at 30 keV. In reality, the membrane could be made even thinner and behaves as a 2D system. As will be shown below, in our nano engineered nanopillar-membrane device, it is precisely the electron-solid interaction within the nanopillars that enhances the overall electron generation. In other words, the surface increase of the 2D-membrane by 1D-nanopillars enhances SEE to a degree where the membrane amplifies the incoming number of electrons more effectively than a 3D system. Thus adding the dimensions 2D+1D as for the nanopillar-membrane system leads to a behavior different from a 3D bulk system.

Fig. 2(a) shows a color-scale map of the anode current (normalized by the incident beam current I_b) as a function of the position of the e-beam scanning over the back side of four membranes. We can directly compare this map with the SEM image shown in Fig. 1(b). We find that the anode signal provides a high contrast in membrane thickness and shows a clear enhancement of electron emission in the area of nanopillars (Δ compared to M). The plot in Fig. 2(b) represents a line scan taken from the corresponding color-scale map. Obviously, one can directly follow transitions between non-membrane area (B), membrane (M) and membrane with nanopillars (Δ).

The origin of enhanced SEE from the nanopillars is further explored by altering the anode voltage. Since the anode with a negative potential will keep electrons with energy below $e|V_a|$ from reaching the anode, it thus provides a method to analyze the energy of emitted electrons by sweeping the anode voltage. The $I_a - V_a$ characteristics in Fig. 3(a) were measured for the three distinct areas (B, M and Δ) for comparison. The anode voltage was swept from -200 V

to +200 V. Constant levels of anode current are observed when $V_a < -150$ V. These levels reflect the contribution from those electrons transmitted through the nanopillar-membrane system where the electrons' energy is only slightly attenuated ($E \leq E_p = 30$ keV). Upon further increasing the anode voltage up to +30 V, a continuous rise in the anode current due to SEE is found. Above $V_a = +30$ V, most transmitted primary and secondary electrons are collected by the anode and the anode current reaches a saturation value. In Fig. 3(a), the black curve shows the electron emission through the non-membrane area (B), which is suppressed in reverse bias to 36% and increased in the forward direction to about 83%. The increase of 47% is the contribution from secondary electrons. Turning now to the signals from the membrane (M) and the nanopillar-membrane system (Δ), we can see the direct transmission of the primary electrons is increased by about 12%, where this increase relates to the thinness of the membrane comparing to the unprocessed multi layers (B). However, the contribution from SEE is increased to 57% for area M and 67% for area Δ . Because of the increase in SEE, the total emission current becomes greater than the incident current, i.e., a gain is achieved.

We found that in contrast to the intuitive assumption – that is the thinner membrane the higher the transmission should be – a membrane with nanopillars shows an even more enhanced signal. As depicted in the inset of Fig. 3(a), the derivative of the Δ -trace with respect to the anode voltage represents the energy distribution of the secondary electrons. We further examined the effects of nanopillars on electron emission by scanning the e-beam (30 keV) across the nanopillar frame at $V_a = \pm 200$ V. Electron emissions from areas B, M and Δ are compared directly in Fig. 3(b). A remarkable influence of the nanopillars (Δ -peaks) is found. Under a forward anode bias $V_a = +200$ V, same as that in Fig. 2(b), an enhancement of SEE by the nanopillars is clearly observed. Under reverse anode bias $V_a = -200$ V transmission of primary electrons is slightly suppressed by the nanopillars, which is also seen in Fig. 3(a) (see the arrows). This is a clear indication that the nanopillars absorb high-energy primary electrons and generate more low-energy secondary electrons than the 2D membrane alone.

This effect also suggests that in order to obtain an optimal SEY the ratio of membrane thickness to nanopillar height and the aspect ratio of nanopillars have to be carefully tuned. Comparing to curve B in Fig. 3(a), it has to be noted that curve M has a stronger dependence on positive anode potential. This is directly related to the fact that the electric field in

the recessed membrane area is retarded (see Fig. 1(a)). Furthermore, the even stronger dependence on anode potential found in area Δ stems from the suppression of the electric field on the nanopillar sidewall by neighboring nanopillars. This suggests that the SEE from a patterned/rough surface could be optimized by an electric field applied so that the reentrance of secondary electrons into neighboring nanopillars is avoided. Furthermore, it is of great interest to explore electron emission from nanopillars at even higher electrical fields where field emission can kick-in and help removing electrons from the nanopillars.

The above results were obtained for the incident energy of 30 keV. The detailed dependence of electron emission on the incident energy is shown in Fig. 4. Again emission signals from areas M and Δ are compared for $V_a = +200$ V. The threshold energy for electrons to 'penetrate' the nanopillar-membrane system is about 12.5 keV. There is no observable shift in the threshold energy comparing areas M and Δ . However, nanopillars significantly increase the emission signal – that is the yield $\gamma = \gamma(\gamma_m, \gamma_p)$ of emitted electrons, where γ_m and γ_p are the yields of SEE for membrane and nanopillars, respectively [14]. The solid line shown in Fig. 4 is a Monte Carlo approximation to the SEE from thin membranes, based on the Bethe model of energy loss and a parametric model of SEE [1, 15, 16]. Above 30 keV, which is the maximal energy available in our SEM, a saturation of the anode current levels is expected.

Above the threshold energy of 12.5 keV, an enhancement of 180% by the nanopillars is obtained as compared to the membrane. The cause for this enhancement obviously is the altered surface morphology due to the nanopillars, which increases the effective surface area and the effective incident angle for electrons (see Monte-Carlo simulation in Fig. 1(f)). It has to be noted that the thickness of current membranes is about 1.6 microns, which is much larger than the penetration depth of 30 keV electrons. A thinner membrane allows more primary electrons to reach the nanopillars and produce more secondary electrons. In the frame of this interpretation, the normalized anode current, defined as the total yield $\gamma = I_a/I_b$, can be expressed as $\gamma = \beta\gamma_p + (1-\beta)\gamma_m$, where β is the coverage of the membrane surface by nanopillars. For an area Δ on this particular device, we have $\beta = \pi d^2/4L^2 \approx 0.13$, where d is the diameter of a nanopillar, and L is the pitch distance. Consequently, a higher SEE can be achieved by decreasing the pitch distance between nanopillars. By reducing the pitch distance from 200 nm to 150 nm, while maintaining the pillar's dimension, β can be doubled. In the current device, the thickness of the membrane is much larger than the mean-

free-path of the incident electrons meaning a large number of incident electrons are slowed down by scattering before they enter into nanopillars. Longer nanopillars will substantially increase both the generation and emission of SEs. A larger diameter for nanopillars increases the emission area, however, it also decreases the possibility for secondary electrons to escape from nanopillars. Hence, there is an optimized diameter corresponding to the energy of incident electrons. When a strong electric field is applied to prevent emitted electrons from being absorbed by neighboring nanopillars, longer nanopillars (but no necessarily longer than the penetration depth) can increase the emission area and hence maximize the SEY. Comparing to the obtained enhancement factor of 1.8 shown in Fig. 4, a factor of 10 in the enhancement of SEE is expectable if a proper optimization of the dimensions can be achieved: a thinner membrane, longer nanopillars, an optimized diameter and pitch distance. With an even higher electric field, field emission of stimulated electrons will take place and dramatically enhance the emission current [17, 18]. A higher yield of SEE can also be realized by choosing a material with higher intrinsic yield of SEE, e.g., diamond [19]. Here, we emphasize that integration of nanopillars on a membrane has two obvious advantages: (i) they naturally provide a boost to SEE by the geometrical change of the emission surface, as we have seen, and (ii) they constitute an array of pointing emitters operating in parallel, which has great potential for including other emission mechanisms such as electron field emission and plasmon/phonon/photon-assisted emission.

In summary we have demonstrated that a nanopillar-membrane system can be engineered and optimized to maximize the SEY. Electron-solid interactions in the world of nano objects will demonstrate new effects and find applications in new-concept devices. Particularly in the device shown here, the functions of the membrane and nanopillars are separated in a sense that the membrane acts as a filter/window for incident particles, while the nanopillars are the true active elements. It is clear that the geometry of the nanopillars and the arrays can be freely chosen. One can use a host of different heterostructure materials, such as *p-n* junctions, quantum wells, etc., to integrate into the nanopillar-membrane system, which further enhances the functionality. Finally, nanopillars can be further configured as electron field emitters, where they serve not only as a host of particle-solid interaction, but also as probes of electronic/mechanical excitations in nanopillar-membrane systems disturbed by incident particles or radiation.

The authors thank Michael S. Westphall and Lloyd M. Smith for helpful discussions

and comments. The authors like to acknowledge support from Wisconsin Alumni Research Foundation (WARF), the National Science Foundation (MRSEC-IRG1), and the Air Force RSO under contract number F49620-03-1-0420.

-
- [1] H. Bruining, *Physics and applications of secondary electron emission*, McGraw-Hill Book Co. Inc, New York (1954).
 - [2] W. L. Wilcock, D. L. Emberson, and B. Weekley, *Nature* **185**, 370(1960).
 - [3] J. B. Johnson, and K. G. McKay, *Phys. Rev.* **93**, 668 (1954).
 - [4] H. Kanter, *Phys. Rev.***121**, 677 (1961).
 - [5] R. F. Egerton, *Electron energy-loss spectroscopy in the electron microscopy*, Plenum Press, New York (1986).
 - [6] L. Stab, *Nucl. Instr. and Meth. A* **288**, 24 (1990).
 - [7] T. Kamiya, M. Cholewa, A. Saint, S. Prawer, G. J. F. Legge, J. E. Butler, and D. J. Jr. Vestyck, *Appl. Phys. Lett.* **71**, 1875 (1997).
 - [8] F. S. Porter, D. McCammon, M. Galeazzi, and C. K. Stahle (Eds.), *Low temperature detectors: Ninth International Workshop on Low Temperature Detectors* , AIP Conference Proceedings **605** (2001).
 - [9] K. Nishimura, T. Itotani T. and K. Ohya, *Jpn. J. Appl. Phys.***33**, 4727 (1994).
 - [10] M. Suzuki, T. Yamada, and C. Y. Yang, *Appl. Phys. Lett.* **90**, 083111 (2007).
 - [11] The total energy of field emitted electrons depends on the anode voltage applied.
 - [12] A. V. Crewe, J. Wall, and J. L. Langmore, *Science* **168**, 1338 (1970).
 - [13] N. D. Browning, M. F. Chisholm, and S. J. Pennycook, *Nature* **366**, 143 (1993).
 - [14] Different to the conventional definition of secondary electron yield, here the yield γ_p and γ_m include both the transmitted electrons and the true secondary electrons.
 - [15] A. Bethe, in *Handbuch der Physik*, Vol. 24 (Verlag Julius Springer, Berlin, 521 (1933).
 - [16] D. C. Joy, *Monte Carlo Modeling for electron microscopy and microanalysis*, Oxford University Press, New York (1995).
 - [17] A. Nojeh, B. Shan, K. Cho, and R. F. W. Pease, *Phys. Rev. Lett.* **96**, 056802 (2006).
 - [18] H. Qin, H. S. Kim, M. S. Westphall, L. M. Lloyd, and R. H. Blick, in preparation, (2007).
 - [19] M. W. Geis, N. N. Efremov, K. E. Krohn, J. C. Twichell, T. M. Lyszczarz, R. Kalish, J. A.

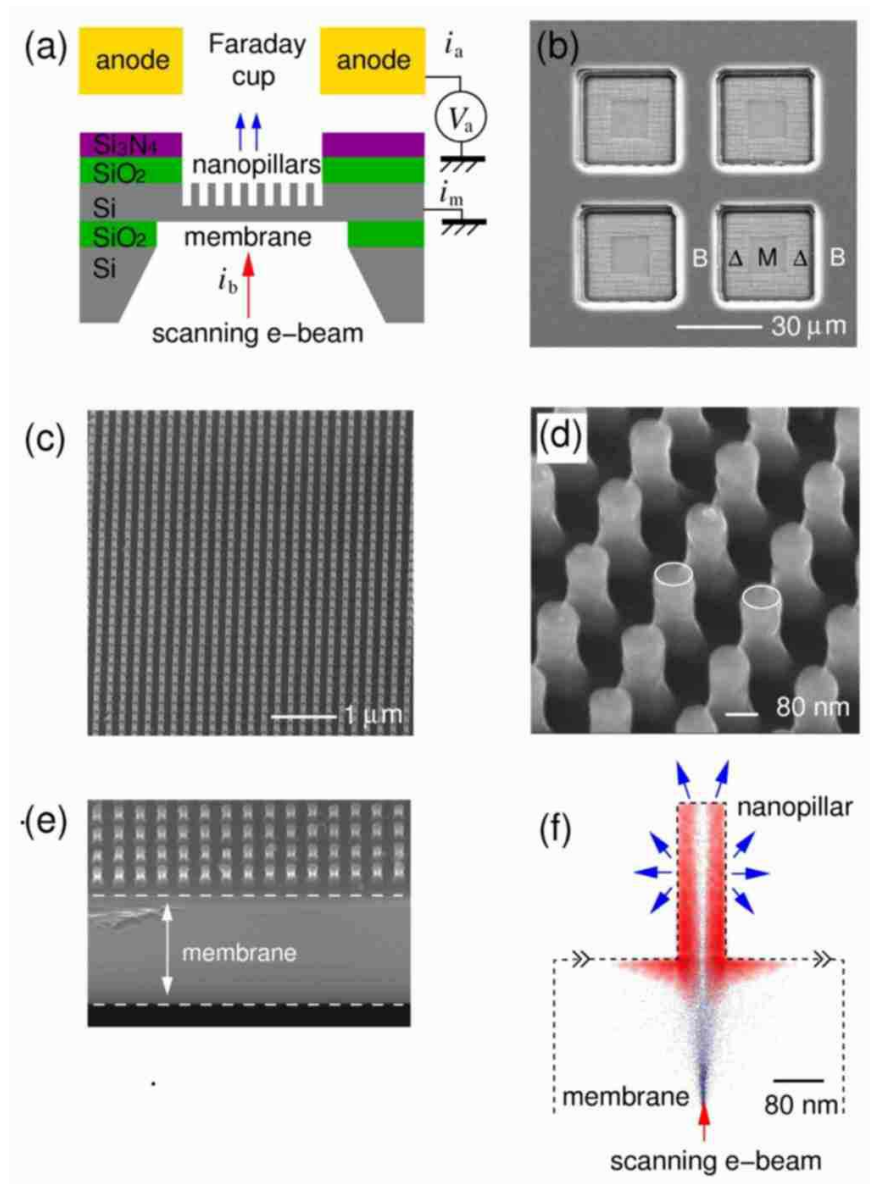
Greer, and M. D. Tabat, *Nature* **393**, 431 (1998).

FIG. 1: Schematics of the device and the experimental setup. The device is a thin silicon membrane with an array of nanopillars fabricated on the top side. (b), (c), (d), and (e) are scanning electron micrographs. (b) A top view of four square membranes. (c) and (d) are close views of a nanopillar array. (e) A cross section of membrane. (f) A Monte-Carlo simulation shows the different distributions of primary electrons (colorized dots) penetrating from beneath and secondary electrons (red color) in a nanopillar-membrane structure (see text for details).

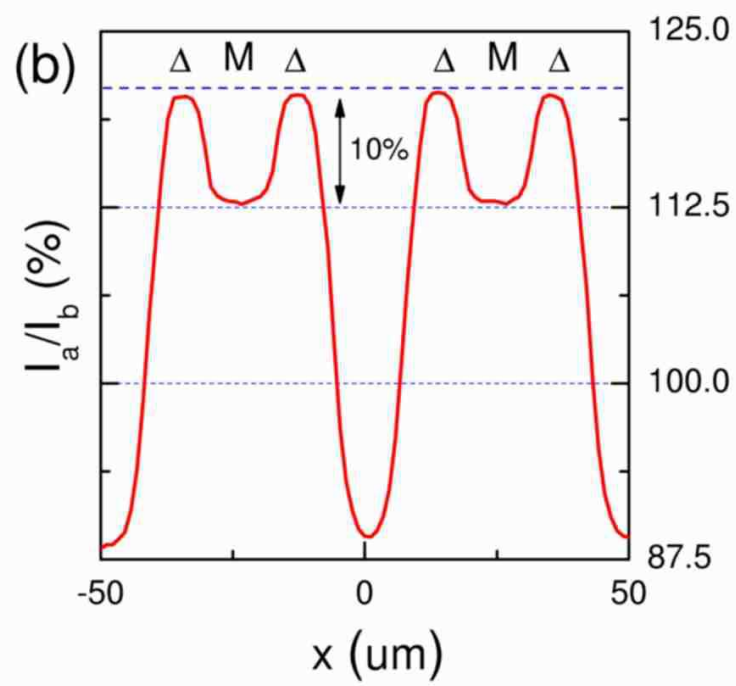
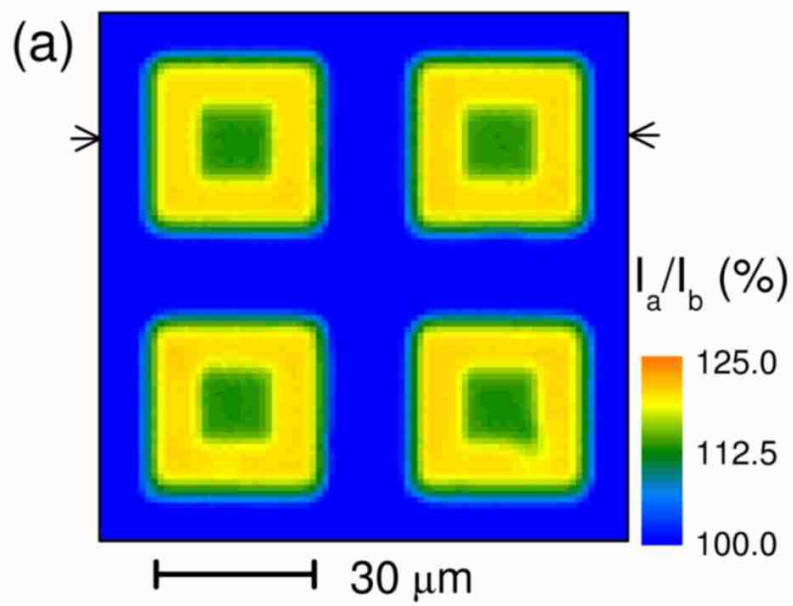
FIG. 2: (a) A color scale plot of anode current as a function of the position of the scanning e-beam. In the experiment, the anode voltage was +200 V. The incident electron energy was 30 keV. The incident e-beam current was set at 200 pA. (b) A line scan taken between the two arrows shown in (a).

FIG. 3: (a) The anode current signals as a function of the anode voltage were probed for comparison when the e-beam was located in areas B, M and Δ . The incident electrons had an energy of 30 keV and the beam current was 200 pA. The inset displays the energy distribution of secondary electrons emitted from area Δ . (b) Two line scans across a single membrane and covering areas B, M and Δ were taken at $V_a = -200$ V and $V_a = +200$ V for comparison. For clarity, the amplitude of the line scan taken at $V_a = -200$ V is multiplied by a factor of 2.

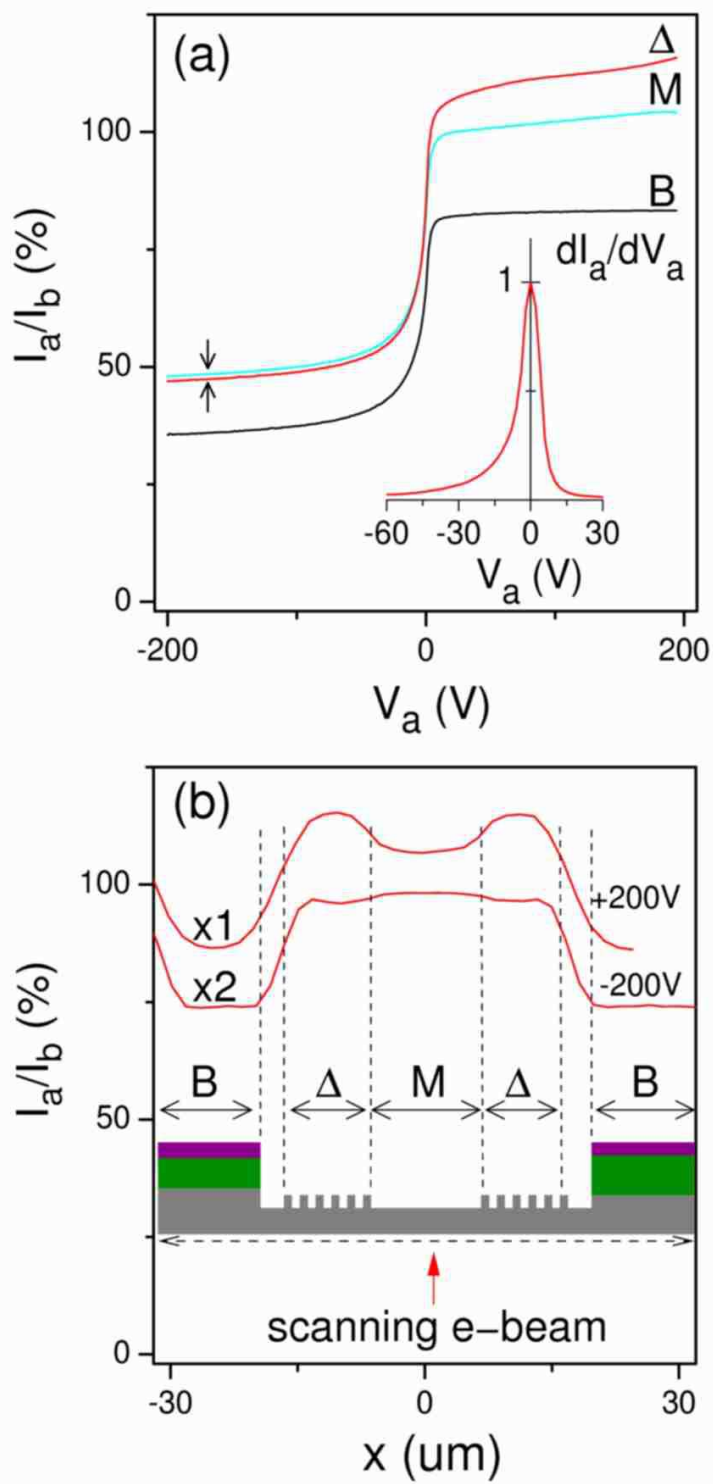
FIG. 4: The dependence of SEY on the incident electron energy is compared for areas M and Δ . The anode voltage was +200 V. The solid line is a Monte Carlo simulation for the membrane.



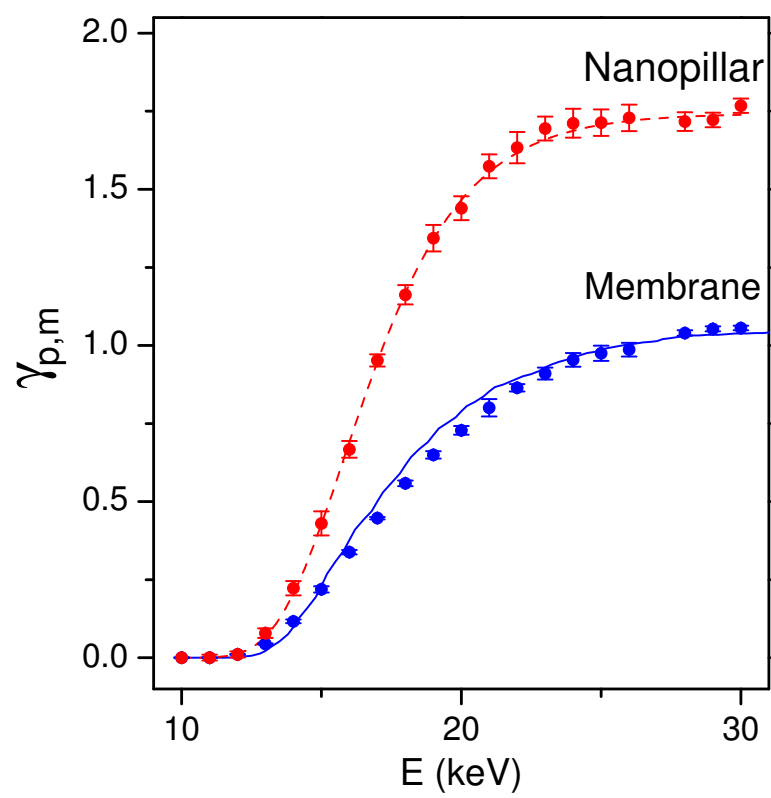
Qin *et al.*: Figure 1/4



Qin *et al.*: Figure 2/4



Qin *et al.*: Figure 3/4



Qin *et al.*: Figure 4/4